

A Bayesian Data-driven Model for Quantifying Electrospray Lifetime

IEPC-2022-230

*Presented at the 37th International Electric Propulsion Conference
Massachusetts Institute of Technology, Cambridge, MA, USA
June 19-23, 2022*

Shehan M. Parmar¹, Adam L. Collins², and Richard E. Wirz³

*Department of Mechanical and Aerospace Engineering,
University of California Los Angeles, Los Angeles, CA 90095, USA*

To mitigate primary electrospray failure mechanisms and improve overall performance, a complete understanding of plume evolution is necessary. To this end, a data-driven modeling framework has been developed to elucidate emission behavior that leads to experimentally observed mass flux and current density profiles. The relevant computational domain explored in this work assumes plume species motion that is dominated by solely external electric fields generated by extractor and accelerator electrodes. Consequently, charged particles with similar charge-specific kinetic energies starting at the same initial positions follow similar trajectories, thereby reducing the parameter space necessary to fully capture possible ion and droplet trajectories propagated in the Plume Region. The physics-based model was emulated by a surrogate model using a polynomial chaos expansion (PCE) to map model inputs to final line-of-sight (LOS) angles. The PCE was evaluated just as a simple, analytical equation to accelerate computational time within a Bayesian inference framework. The unknown distribution in upstream input conditions for plume species emission angles was quantified with uncertainty bounds, showing the need for super-Gaussian-like distributions similar to downstream mass flux profiles. Initial findings from Gaussian mixture modeling (GMM) show the existence of latent, sub-profiles within a super-Gaussian profile, indicative of dissimilar species created upon emission.

I. Nomenclature

\vec{E}_{ext}	=	external electric field from electrospray electrodes
ϕ_{ext}	=	potential field from electrospray electrodes
V_{jet}	=	voltage at electrospray jet tip
$V_{emitter}$	=	voltage of electrospray emitter
ϕ_{ext}	=	potential field from electrospray electrodes
θ_i	=	initial line-of-sight angle of charged particle
θ_f	=	final line-of-sight angle of charged particle
r_i	=	initial radial position of charged particle
r_f	=	final radial position of charged particle
z_i	=	initial axial position of charged particle
z_f	=	final axial position of charged particle
s_i	=	initial speed of charged particle
s_f	=	final speed of charged particle

¹Ph.D. Student, Mechanical and Aerospace Engineering, 420 Westwood Plaza, Los Angeles, CA, parmar@ucla.edu

²Project Scientist, Mechanical and Aerospace Engineering, 420 Westwood Plaza, Los Angeles, CA, collinsalc55@ucla.edu

³Professor, Mechanical and Aerospace Engineering, 420 Westwood Plaza, Los Angeles, CA, wirz@ucla.edu

γ_i	= initial emission angle of charged particle
γ_f	= final emission angle of charged particle
ρ	= propellant density
K	= propellant conductivity
Q	= flow rate
$\dot{m}(\theta)$	= angular distribution of mass flux
$\dot{m}(\theta)_{loss}$	= mass impingement on grids
θ_{crit}	= grid line-of-site angle
t_{sat}	= grid saturation time (i.e., electrospray end of life)
$\left(\frac{q}{m}\right)_i$	= specific charge of charged particle i
S_i	= Sobol index for variable i

II. Introduction

Electrosprays emit charged droplets by applying a strong electric field onto a highly-conductive ionic liquid to generate thrust. Success of future space missions such as the Laser Interferometer Space Antenna (LISA) and the Habitable Exoplanet Observatory (HabEx) [1–5], rely on electrospray thrusters to achieve low thrust-noise, high thrust-precision, and long duration capabilities. Onboard the recent LISA Pathfinder mission, the Colloid MicroNewton Thruster (CMNT) developed by Busek Co., Inc. and NASA Jet Propulsion Laboratory (JPL) demonstrated thruster lifetimes of approximately 2400 hours. [2] Thus, there is a clear technological need for improved electrospray lifetime in order to achieve nominal requirements of $\sim 40,000$ hours for the LISA mission, for instance [6].

In previous work, Thuppul et al. [7] concluded overspray as the primary failure mechanism most influenced by thruster design considerations (e.g., operation and control, geometry, and material and propellant selection) [2, 7]. Overspray is defined as any emitted propellant directed towards the grids, or electrodes, of an electrospray, resulting in eventual saturation of the grids as well as induced secondary failure mechanisms including backspray and insulator wetting. Therefore, reducing mass flux directed to extractor and accelerator grids is critical for improving electrospray lifetime.

Consequently, accurate lifetime predictions require a better understanding of extraction and electrospray plume evolution mechanisms that influence mass flux to the grids. While previous retarding potential [8] and plume divergence angle [1] measurements have shown current density profiles of electrospray emission that follow Gaussian-like distributions, no evidence suggests that corresponding mass flux profiles follow the same distribution due to polydisperse plume profiles [7]. Recent characterization of electrospray plumes at the University of California, Los Angeles (UCLA) Plasma, Energy, & Space Propulsion Laboratory (PESPL) have also shown dissimilar mass flux and current density profiles in shape and width highlighted by quartz crystal microbalance (QCM) measurements [9]. Moreover, downstream plume profiles have an apparent, super-Gaussian functional form where massive species are detected out at high half-angles up to at least 40° . Resolving mass flux at such high angles becomes especially important since small deviations in plume profile shape can propagate into large uncertainties in expected lifetime.

To examine the underlying source of experimentally observed mass flux profiles, high-fidelity computational models are desired to ascertain the initial conditions that result in, for example, a super-Gaussian plume shape. It is known that the relevant physics-based phenomena for electrospray propulsion span multiple length and time scales: nanodroplet breakup [10] induced by ion evaporation [11–13] or Coulombic fission [14, 15], inter-droplet Coulomb interactions or space-charge [16–18], and cone-jet formation and extraction [19, 20]. Furthermore, secondary species emission (SSE) during droplet-mode electrospray operation must also be considered when validating models against measurements taken in vacuum test facilities [21]. To this end, the UCLA PESPL has discretized the electrospray computational domain into multiple regions, each modeled by their most dominant physics- or chemistry-based phenomena, as shown in Figure 1 [22].

The present study focuses on the Plume (or Exhaust) Region, where space charge effects can be considered negligible and plume evolution is dominated solely by applied electrostatic forces. The Propagation of Electrospray Plume Particles in the Exhaust Region (PEPPER) model serves as a reduced-order model capable of rapidly exploring the parameter space of interest. The PEPPER model is uniquely positioned in the computational domain to accept inputs from the Interaction Region, where the UCLA PESPL Discrete Electrospray Lagrangian Interaction (DELI) model can capture critical, inter-droplet Coulomb forces induced by negative velocity gradients among inhomogeneous charged droplet species [18]. The primary objective of this model is to determine the initial conditions that generate mass flux and

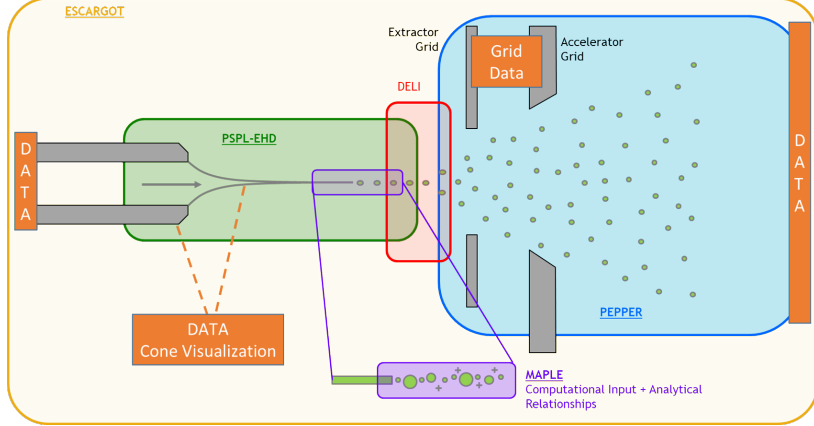


Fig. 1 UCLA PESPL Discretized Electrospray Computational Domain

current density plume profiles observed in previous studies by implementing a robust, data-driven framework. In this paper, the first section begins by outlining the proposed data-driven modeling framework involving a physics-based model that is captured by a computationally efficient surrogate for efficient Bayesian inference analysis. In the second section, we provide results from both the physics-based and surrogate models that result in inferred emission-site input conditions for the UCLA PESPL electrospray thruster domain. The final section provides a discussion on the electrospray lifetime and performance implications learned from this framework.

III. Data-driven Modeling Methods

The overall goal of the PEPPER modeling framework is to solve a canonical inverse problem by which unknown multi-dimensional, model parameters are quantified based on a set of observations. Inverse problems have become a popular method for image denoising [23], climate and geophysical modeling [24], and investigating effects of facility background pressure on electric propulsion system performance [25]. Formally, an inverse problem is defined by

$$g = \mathbb{M}(f) + \epsilon, \quad (1)$$

where some measured data, $g \in Y$, is the result of the forward problem where model parameters $f \in X$ are mapped by some operator, \mathbb{M} , within the confines of observational noise, $\epsilon \in Y$ [23]. Inverse problems commonly invoke Bayesian inference and surrogate modeling approaches to rigorously evaluate model parameter uncertainty and reduce computational time. The PEPPER modeling framework employs such methods in lieu of high-fidelity, numerical simulations. The following section describes the physics-based model, the subsequent generation of a surrogate model, and the Bayesian inference approach to investigate electrospray emission behavior.

A. Plume Modeling Theory

Conclusions from high-fidelity plume models show that inter-droplet Coulomb interactions [16, 26], as charged particles escape an initial, “critical” region or interaction region [18] a certain distance away from the electrospray emitter, the external electric field, \vec{E}_{ext} , generated by the electrodes dominates over Coulomb interactions. The resulting equations of motion are thus

$$\frac{d^2\vec{x}_i}{dt^2} = - \left(\frac{q}{m} \right)_i \nabla \phi_{ext} = \left(\frac{q}{m} \right)_i \vec{E}_{ext}, \quad (2)$$

where \vec{x}_i is the position of particle i , $\left(\frac{q}{m} \right)_i$ is the particle’s specific charge, and ϕ_{ext} is the potential field from the external boundary conditions at the emitter and extractor electrode.

Figure 2 depicts a typical trajectory of a plume particle and the most pertinent variables. To solve for the final radial and axial positions, r_f and z_f , in the Plume Region, the particle’s initial emission characteristics must be known, namely the radial and axial positions, r_i and z_i , initial velocity magnitude and angle, s_i and γ_i , and species specific charge.

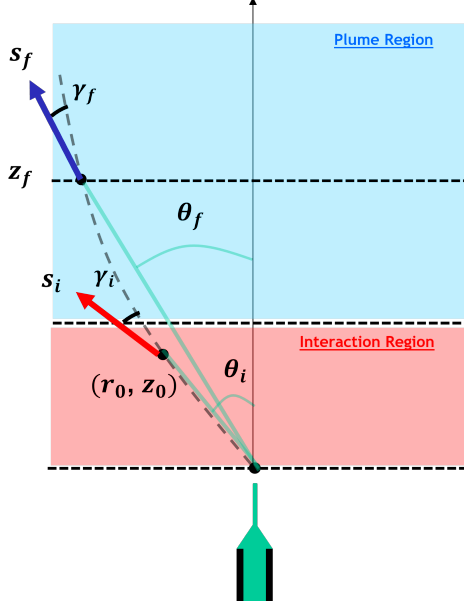


Fig. 2 Baseline trajectory of a typical particle starting from entering the Interaction Region at the emission site z_i , entering the Plume Region, and ultimately exiting a plane of interest at z_f . The trajectory is defined in terms of particle height z , speed s , direction γ , and line-of-sight angle θ .

The initial conditions needed to solve Eqn. 2 are considered unknown. This presents a challenge when estimating the initial distribution of $\left(\frac{q}{m}\right)_i$, for instance. While the disparity in mass flux and charge density profiles are representative of non-uniform specific charge distributions, (i.e., $\frac{q}{m}(\theta)$), the mass flux profile measurements are obtained based on *all* massive species striking the QCM. Despite the lack of detailed resolution of species composition, an invariant property of charged particle motion can be invoked to reduce the unknown variables in this analysis. For charged particles entering a domain with a constant, uniform electric field, any species with the same potential at the emission site, defined by the difference between the jet tip and emitter voltage,

$$V_{jet} - V_{emitter} = \frac{1}{2} \left(\frac{m}{q} \right)_i \vec{v}_i^2, \quad (3)$$

will follow the same trajectory so long as the initial positions remain the same. In the simplest case, where the emission potential is set to zero, particle trajectories follow a straight line along the z -axis, irrespective of species specific charge. Perturbations to this value result in families of similar trajectory curves. Thus, particles initialized in the Plume Region domain are set with constant values of charge-specific initial kinetic energies, where $\frac{1}{2} \left(\frac{m}{q} \right)_i s_i^2$ is estimated using retarding potential analyzer (RPA) measurements for a specified flow rate Q , beam current I_B , and ionic liquid propellant, 1-ethyl-3-methylimidazolium bis(trifluoromethylsulfonyl) imide (EMI-Im) [27, 28]. Based on well-known scaling laws, Q and the propellant conductivity K can provide an estimated particle mass, shown in Eqn. 4,

$$m_i = \rho \frac{\pi}{6} \left(\frac{\epsilon_0 Q}{K} \right), \quad (4)$$

where ρ is the propellant density, ϵ_0 is the vacuum permittivity, and droplet diameter is defined by $d = (\epsilon_0 Q / K)^{\frac{1}{3}}$ [29]. It follows that the initial position θ_i and emission angle of the species γ_i are the remaining unknown variables to determine a plume particle trajectory. Previous sensitivity analyses have shown that γ_i is the most influential variable that controls overall radial plume expansion [30]. The subsequent sections will outline the data-driven modeling framework used to infer the most probable initial distribution in $f(\gamma_i)$ based on experimental mass flux and current density profile measurements.

Based on an initial distribution of charged particles emitted into the Plume Region domain, the subsequent distribution

of final positions in the form of $f(\theta_f)$ can be resolved for some defined downstream plane of interest, z_f . Using the analytical life model defined by Thuppul et al. [7], the mass flux profile can be defined by Eqn. 5 [7],

$$\dot{m}(\theta_f) = \frac{Q\rho}{F_{full}} f(\theta_f), \text{ where } F_{full} = \int_0^\pi 2\pi \sin \theta f(\theta_f) d\theta. \quad (5)$$

The time it takes for the grids to be fully saturated to the point of failure, t_{sat} , is then defined by Eqn. 6

$$t_{sat} = \frac{\rho V_{crit}}{\dot{m}_{loss}}, \quad (6)$$

where V_{crit} is the accumulated propellant volume saturating the grid. The rate of mass impingement on the grid is defined by Eqn. 7,

$$\dot{m}_{loss} = 2\pi \int_{\theta_{crit}}^{\frac{\pi}{2}} \dot{m}(\theta_f) \sin \theta d\theta, \quad (7)$$

where θ_{crit} is the grid line-of-sight angle with respect to the emission site [7]. To perform this analysis, a computational model was built in the COMSOL Multiphysics software, version 5.6 to solve for the electric field and simulate charged particle trajectories.

B. Surrogate Model

As the dimensionality of the model parameters increase, inverse problems generally benefit from a reduced-order forward model. As described above, the primary input parameters, $f \in X$, needed to solve for the particle's trajectory are the initial positions, θ_i , initial emission angles, γ_i , and the geometry-dependent variables, such as the $V_{electrode}$. If each of these input variables are assumed to be unknown, we would like to generate a computationally inexpensive method to explore a possibly large functional design space. Thus, a model surrogate, or “metamodel”, defined by some arbitrary analytical function $Y = \mathbb{M}(\vec{X})$ can be defined to map the relevant inputs to the output of interest, as defined by Eqn. 8,

$$\mathbb{M} : \theta_i, \gamma_i, V_{electrode} \rightarrow \theta_f, \quad (8)$$

where \vec{X} denotes each of the input variables.

For a low-dimensional set of model parameters, simple nth-order polynomial functions can be used. Concretely, rapid assessment of final particle positions can be expressed as

$$\mathbb{M}(r, z) = \sum_{i,j}^n C_{ij} r^i z^j, \quad (9)$$

where C_{ij} are the model coefficients.

As model parameters increase (i.e., including extractor and accelerator electrode potentials, domain geometry modifications, or weighted, multi-component emission profiles) the functional form of a polynomial chaos expansion (PCE) is more suitable and has been successfully applied to numerous multi-dimensional engineering problems. [31–34] Its respective functional form is shown in Eqn. 10,

$$\mathbb{M}(\vec{X}) = \sum_{\alpha \in \mathbb{N}^d} y_\alpha \Psi_\alpha(\vec{X}), \quad (10)$$

where a basis set of multivariate, orthogonal, Hermite polynomials, $\{\Psi_\alpha(\vec{X}), \alpha \in \mathbb{N}^d\}$, is bounded by the dimension d of the input parameter space \vec{X} . Each polynomial, or “mode”, is weighted by coefficient y_α to generate the entire PCE function. The coefficients y_α are determined using a standard regression procedure by first obtaining results from the physics-based computational model (i.e., charged particle tracing in COMSOL). For the following analysis, the input parameter space is sampled using Latin hypercube sampling [35]. Both sampling and regression methods are implemented using an open-source Python package, Chaospy [36]. The resulting model surrogate resolves the final position of the particle using a single analytical equation.

C. Bayesian Inference

Eqn. 8 enables rapid evaluation of arbitrary distributions in each of the individual variables. In order to determine the uncertain variables, a Bayesian inference approach becomes a suitable method of analysis. The goal of Bayesian inference is to generate a posterior distribution for a series of hypotheses [37]. Bayes' theorem is comprised of two terms, the likelihood function and prior distribution, shown in the right-hand side of Eqn. 11

$$\text{prob}(\theta_i, \gamma_i | \dot{m}(\theta)_{UCLA-QCM}, I) \propto \text{prob}(\dot{m}(\theta)_{UCLA-QCM} | \theta_i, \gamma_i, I) \cdot \text{prob}(\theta_i, \gamma_i | I), \quad (11)$$

where θ_i and γ_i are the uncertain parameters, or hypotheses, we wish to quantify (assuming some constant $V_{electrode}$), $\dot{m}(\theta)_{UCLA-QCM}$ denotes the available mass flux profile measurements provided by UCLA PESPL QCM results, and I represents background knowledge. It is assumed that each data measurement is distributed normally with an assigned, finite variance. The posterior distribution is solved by implementing a Hamiltonian Monte Carlo (HMC) No U-Turn Sampling technique using an open-source Bayesian inference Python tool, PyMC3 [38]. In this way, the unknown variables can be directly quantified and bounded by uncertainty envelopes to determine a set of initial conditions near the site of electrospray emission that lead to the experimentally observed, super-Gaussian mass flux profiles [9].

The likelihood function was selected based on the functional form of experimental observations (i.e., Gaussian to super-Gaussian),

$$\text{prob}(\dot{m}(\theta)_{UCLA} | \theta_i, \gamma_i, V_{electrode}, I) = \prod_i^N \text{prob}(\dot{m}(\theta)_i | \theta_i, \gamma_i, V_{electrode}, I) \quad (12)$$

where the $\dot{m}(\theta)_i$ is estimated by plugging the distribution $f(\theta_f) = \mathbb{M}(f(\theta_i) = 0, \gamma_i, V_{electrode} = 4.4\text{kV})$ into analytic equations that produce mass flux. In this preliminary study, the same analysis is conducted as was done in previous work, were only the unknown parameters in the emission angle are observed,

$$f(\gamma_i) = A \exp\left(-\left(\frac{(\gamma - \mu)^2}{2\sigma^2}\right)^n\right). \quad (13)$$

The profile amplitude, A , width, σ , tilt, μ , and sharpness, n , are physically-motivated parameters that will elucidate the emission behavior of an electrospray system. The complete equation for a single sample $\dot{m}(\theta)$ is shown in Eqn. 14:

$$\begin{aligned} \dot{m}(\theta)_i &= \frac{Q\rho}{F_{full}} f(\theta_f), \\ \text{where } F_{full} &= \int_0^\pi 2\pi \sin \theta f(\theta_f) d\theta, \\ \text{where } f(\theta_f) &= \mathbb{M}\left(\left[A \exp\left(-\left(\frac{(\gamma - \mu)^2}{2\sigma^2}\right)^n\right)\right], \theta_i, V_{electrode}\right), \\ \text{where } \mathbb{M}(\vec{X}) &= \sum_{\alpha \in \mathbb{N}^d} y_\alpha \Psi_\alpha(\vec{X}), \end{aligned} \quad (14)$$

where the polynomial chaos expansion (PCE) (c.f., kernel function) in \mathbb{M} is composed of a basis set of multivariate, orthogonal polynomials, $\{\Psi_\alpha(\vec{X}), \alpha \in \mathbb{N}^d\}$, and is bounded by the dimension d of the input parameter space \vec{X} . To efficiently sample posterior distributions, a custom gradient class for PCEs was developed in Python. This is because in order to use the Hamiltonian Monte Carlo (HMC) No U-Turn Sampling technique offered by PyMC3, the gradient must be known; Eq. 14 is a complex function and basic, univariate slice sampler step methods are prohibitively slow.

IV. Results

A. Charged Particle Tracing Reduced Order Model

Charged particle trajectories are solved using the COMSOL Multiphysics Electric Field Solver and Charged Particle Tracing module. The potential field is shown in Figure 3 for an electrospray domain representative of the experimental conditions at the UCLA PSPL.

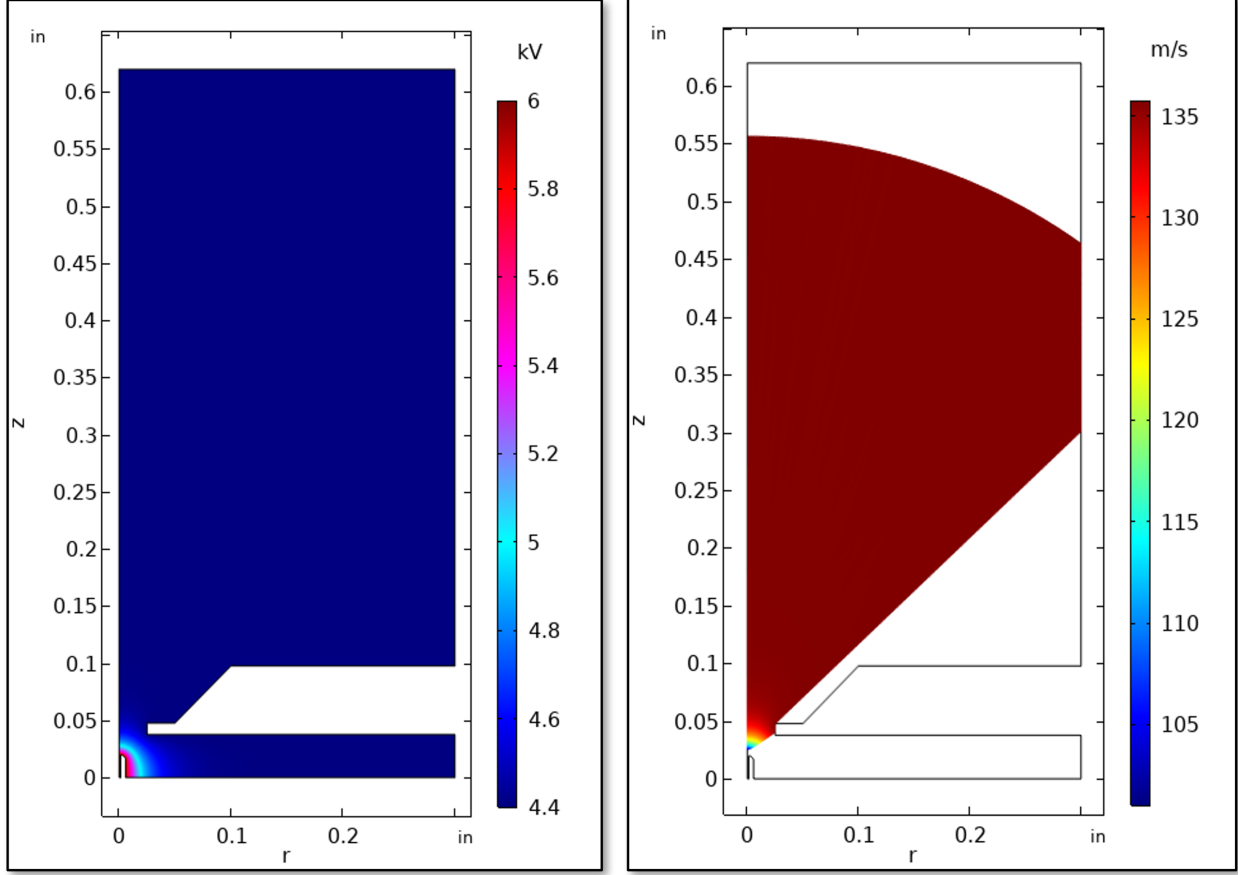


Fig. 3 Potential field solution (left) of electrospray geometry with an extractor electrode and particle trajectory sweep (right) over representative γ_i values.

Figure 3 illustrates the plume particle trajectories using an initial parameter sweep over representative values for γ_i . Initial conditions for the kinetic energy to charge ratio were set to be on the order of ~ 1000 V to match experimental RPA results for droplet-mode electrospray emission using EMI-Im propellant [27, 28]. The particle trajectories were used in a standard regression procedure to obtain the coefficients for Eqns. 9 and 10. Figure 4 shows the solution space over particles with various initial charge-specific kinetic energies and a 3rd-order polynomial fit. By producing a similar series of functions for both a domain with and without an accelerator electrode, rapid assessment of changes in final line-of-sight angles is made possible, as shown in Figure 5.

B. Inverse Problem and Inference

Following Eqn. 11, a likelihood function was selected based on the functional form of experimental observations (i.e., Gaussian to super-Gaussian),

$$\text{prob}(\dot{m}(\theta)_{UCLA-QCM} | \theta_i, \gamma_i, I) = \prod_i^N \text{prob}(\dot{m}(\theta)_i | \theta_i, \gamma_i, I) \quad (15)$$

where the $\dot{m}(\theta)_i$ is estimated by applying $f(\theta_f) = \mathbb{M}(f(\gamma_i), \theta_i = 0, V_{\text{electrode}} = 4.4 \text{ kV})$ to Eqn. 5. The unknown parameters are found in the distribution of emission angles,

$$f(\gamma_i) = A \exp\left(-\left(\frac{(\gamma - \mu)^2}{2\sigma^2}\right)^n\right). \quad (16)$$

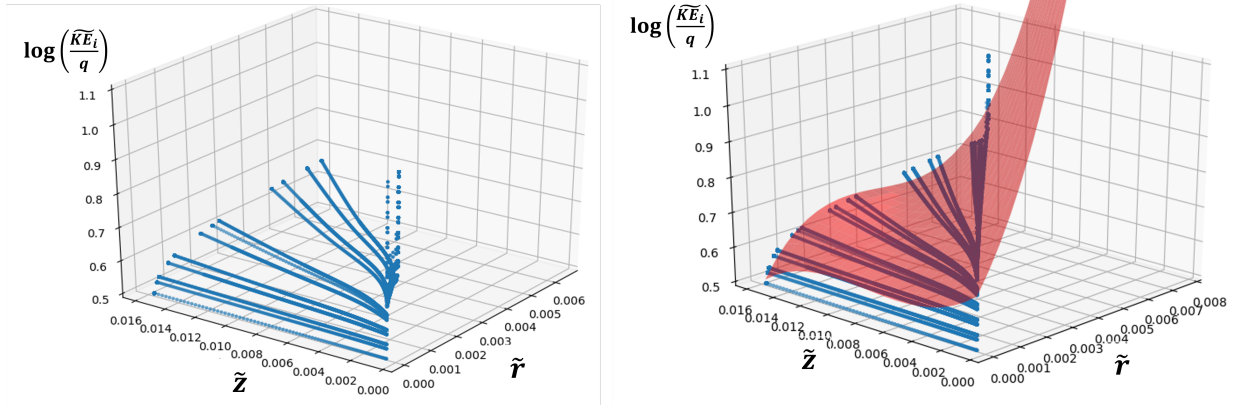


Fig. 4 (Left) Example of polynomial function used to map particle initial positions (r_0 and z_0) and initial $\frac{KE}{q}$ for high emission angles of $\gamma_i = 58^\circ$ to final positions. (Right) 3rd-order polynomial fit, $M(r, z)$, shown by red surface.

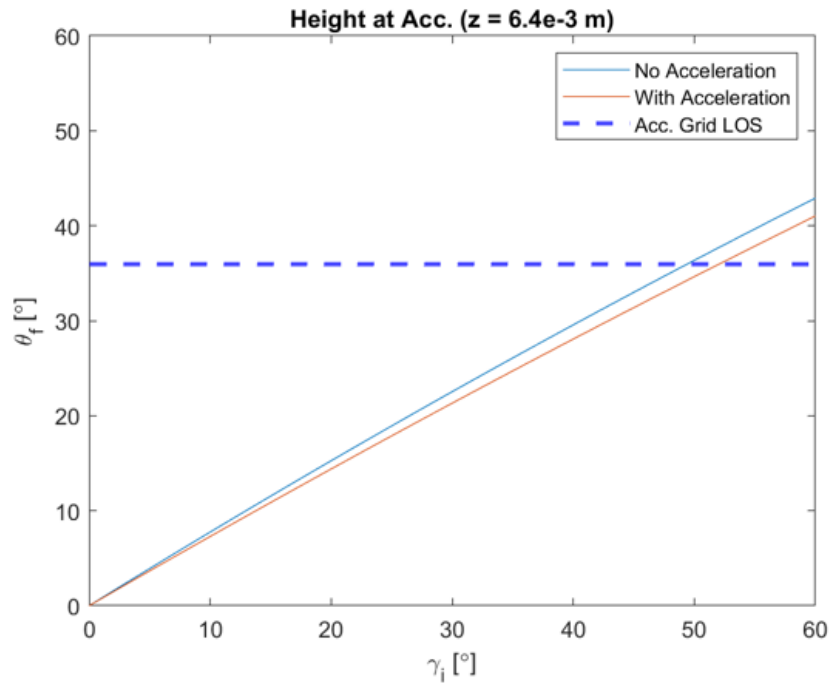


Fig. 5 Change in final line-of-sight angle of particles entering extractor vs. accelerated domain.

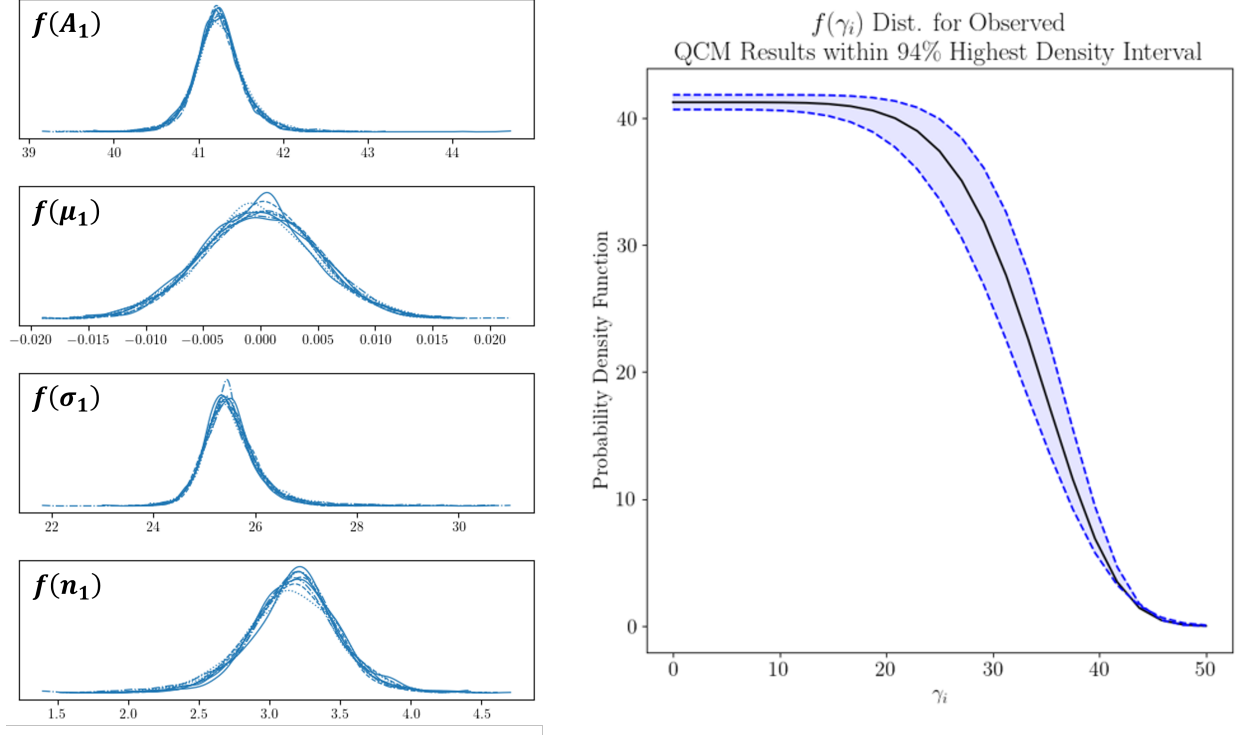


Fig. 6 Posterior distributions (left) for unknown parameters in emission angle distribution, including amplitude, A_1 , tilt, μ_1 , width, σ_1 , and sharpness n_1 and initial emission angle distribution, $f(\gamma_i)$, at emission site (right).

Thus, the likelihood function preserves physically-informed unknown parameters that describe a plume profile at any location downstream of the emission site, including the profile amplitude, A , width, σ , tilt, μ , and sharpness, n . The prior distributions were selected as normal distributions and are shown for each variable in Eqn. 17:

$$A_1 \sim \mathcal{N}(200, 100); \mu_1 \sim \mathcal{N}(0, 10^{-3}); \sigma_1 \sim \mathcal{N}(100, 50); n_1 \sim \mathcal{N}(1.5, 1). \quad (17)$$

After taking 1500 HMC samples, the resulting posterior distributions are shown in Figure 6 along with the corresponding trace plots. The posteriors of each uncertain parameter can be used to show the resulting emission angle distribution defined in Eqn. 16, shown in Figure 6. This plot provides the shape and form of the initial distribution in emission angles that match with the experimental data.

V. Discussion

The results provided in Section IV establish a framework to iteratively model uncertain emission behavior using a combination of data-driven and reduced-order methods. The posterior distributions of model parameters elucidate the fundamental nature of mass flux measurements at the UCLA PESPL. The posterior distributions in Figure 6 resulted in predicted mass flux profiles showing 94% confidence envelopes, shown in Figure 7.

The similarity in profile shape indicates the requirement for super-Gaussian upstream conditions to generate super-Gaussian downstream for electrospray plume evolution governed solely by the external electric field. Moreover, the uncertainty in mass flux predictions show regions of higher uncertainty at high angles. These regions of uncertainty are most consequential to lifetime and performance predictions due to its implications of overspray [7].

A. Mixture Modeling

The results from Section 6 indicate that particles governed solely by the external electric field must emit downstream following a super-Gaussian emission angle profile. Limited theoretical backing for initial generation of a super-Gaussian plume suggests that additional terms may be necessary in the equations of motion to describe emission characteristics.

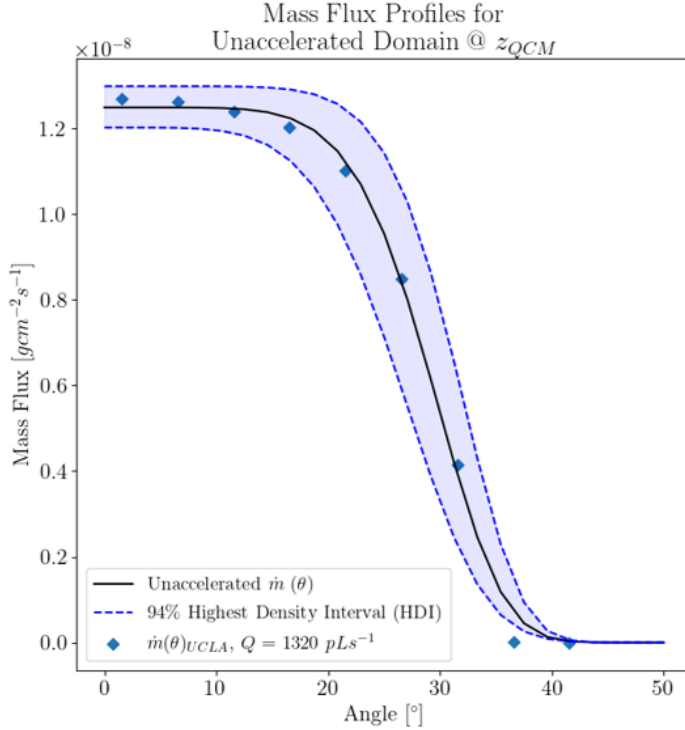


Fig. 7 Model-predicted mass flux profiles via $\vec{M}(\vec{X})$, where $f(\gamma_i)$ from Figure 6 is included in \vec{X} .

For instance, the source of nonlinear inter-particle interactions and collisions may contribute to the non-Gaussian behavior of the *upstream* plume, including Coulomb interactions, ion evaporation, and fission physics may be necessary terms to include in the overall model. The polydispersity of the plume is unknown and greater details regarding the evolved species downstream are desirable. Moreover, in order to predict thrust, neutrally-charged particles also need to be identified.

By inspecting Figure 6, it is hypothesized that a latent variable exists that can allow further investigation of $f(\gamma_i)$. We employ a missing data formulation typically used in mixture modeling, whereby a convolution of multiple Gaussian distributions can model an arbitrary n -order distribution (e.g., super-Gaussian) [39–41]. This method is referred to as Gaussian mixture model (GMM), where the original likelihood function in Eqn. 15 is modified to

$$L(\alpha, \vec{X}, I) = \prod_i^N [\alpha_1 f(\dot{m}(\theta)_i; x_1, I) + \dots + \alpha_k f(\dot{m}(\theta)_i; x_k, I)] \quad (18)$$

where it is assumed that the overarching dataset or training set is derived from a sum of k individual Gaussian distributions weighted by $\alpha_i \in [0, 1]$. This has proven to be especially useful for a variety of applications including GMMs computer vision tasks like multiresolution image representation and reconstruction [42] and high energy physics data classification [43]. Recent work has also achieved filtering out the least significant variables to optimize GMMs for high-dimensional and sparse data sets [44].

Consequently, the breadth of work in GMMs makes it very well suited for the problem at hand: how can the hypothesis of different species compositions at the emission site be made to agree with mass flux experimental observations? Thus, the task of the Gaussian mixture model is to reliably find a combination of finite Gaussian distributions that can produce a similar distribution as in Figure 6. The “clusters” of Gaussian distributions were set to various finite values. Based on axisymmetric linear stability analyses [28, 45] for high-conductivity propellants, it is plausible to assume an electrospray plume is composed of at least primary and satellite droplets that experience angular separation from the original emission site. Thus, we deconvolve the $f(\gamma_i)$ distribution with $k \geq 3$ clusters.

The cluster weights were set by Dirichlet distributions and were ensured to have same number of data points

generated by the inverse transform sampling algorithm. The clusters were then normally distributed and the NUTS algorithm was used for mixing. A primary challenge with this implementation was the long run times for drawing the posteriors since the latent clusters required large sampling and resulted in slow mixing. The resulting weights, α and means are displayed in Figure 9 after using a super-Gaussian data generating process with $n = 10^5$ data points and 1000 samples drawn.

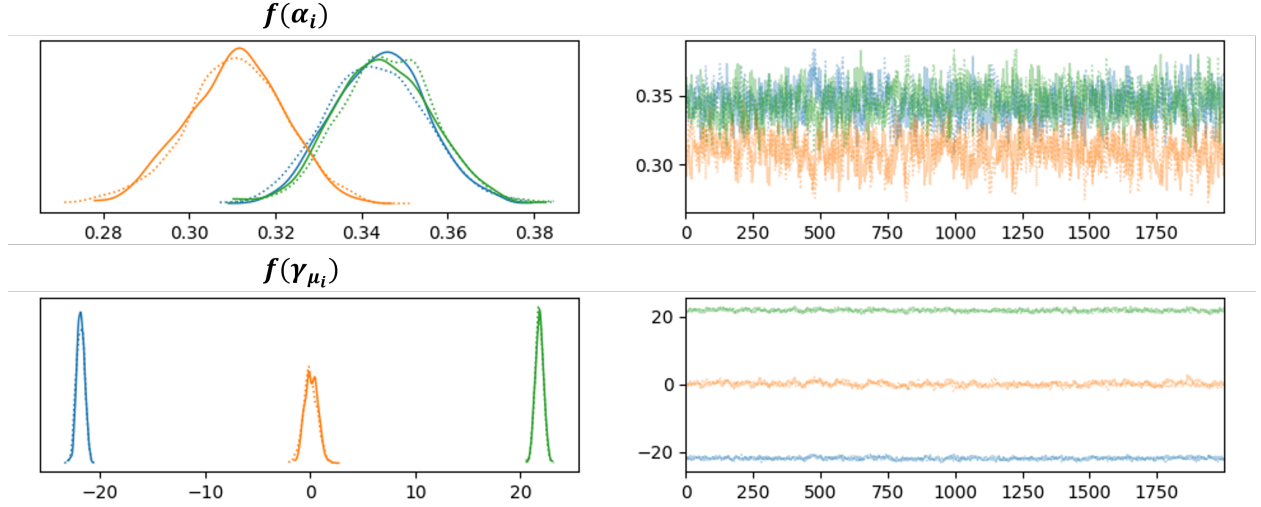


Fig. 8 (Left) Posterior distributions of weighting parameter, α , and mean, μ , of individual Gaussian sub-components of $f(\gamma_i)$ and (Right) the respective trace plot to show each calculated posterior.

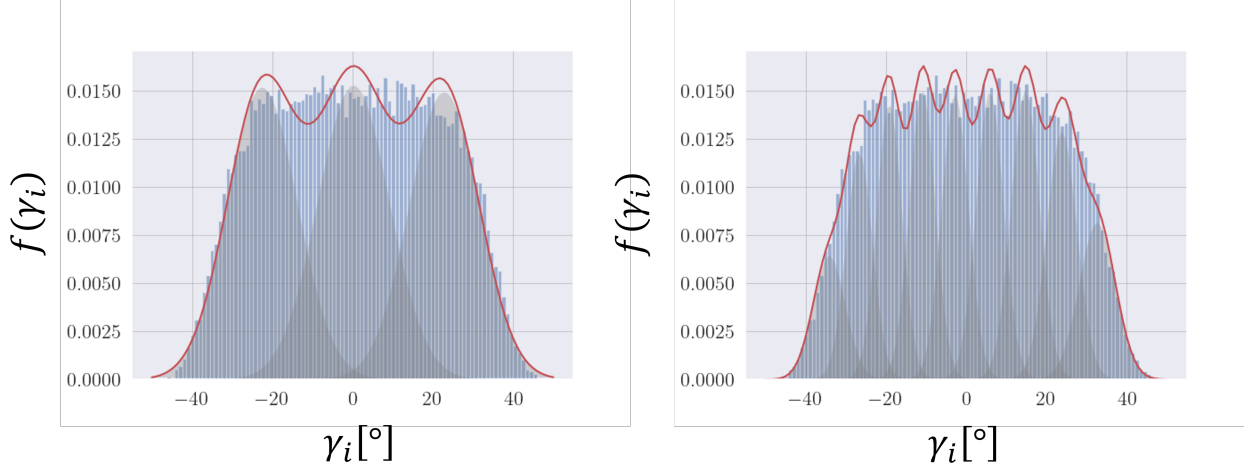


Fig. 9 Sum of 3 (left) and 9 (right) weighted Gaussian mixtures to recapture $f(\gamma_i)$ from Figure 6.

To address overfitting, the Bayesian (BIC) and Akaike (AIC) information criteria in Eqns. 19 and 20 were applied to penalize for increasingly large number of Gaussian components,

$$BIC = -2 \log(\hat{L}) + \log(N)k, \quad (19)$$

$$AIC = -2 \log(\hat{L}) + 2k, \quad (20)$$

where \hat{L} is the maximized likelihood value from Eqn. 18. The BIC and AIC metrics in Figure 10 indicate that $k = 3 - 4$ distributions are most appropriate. Future work aims to modify the penalty term to more appropriately assess the Gaussian mixtures representing emission physics.

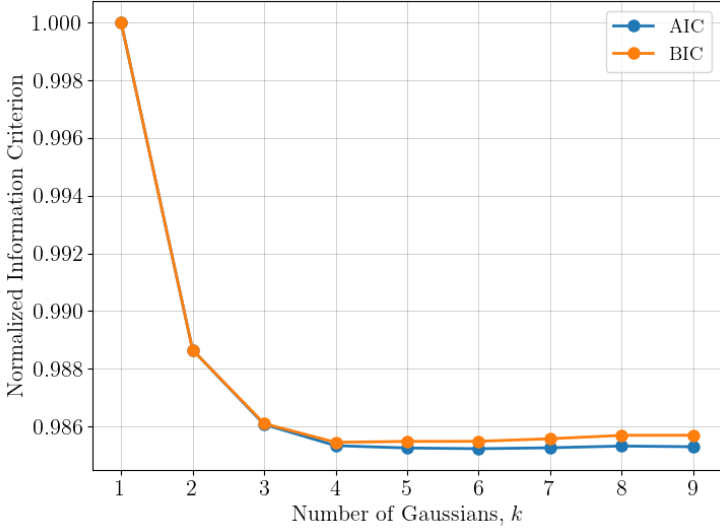


Fig. 10 Bayesian and Akaike information criterion to assess penalty on increased number of clusters versus generality of mixture.

Generalizing downstream profiles with sub-component distributions of arbitrary species is a promising modeling capability. Previous experimental observations of electrospray plume profiles show evidence of polydispersity because the disparate mass flux and current density distributions [9]. Recent Retarding Potential Mass Analyzer (RPMA) experiments also indicate a distribution of disparate species [46]. We hypothesize that physical mechanisms near the emission site, such as fragmentation or fission, result in a multi-source, multi-species upstream emission profile consistent with the GMM results. Furthermore, recent scanning electron microscopy (SEM) images of plume deposition patterns on a nickel foam electrospray beam target further substantiate the advantage of modeling mixtures particle distributions [47, 48]. It was found that foam ligaments displayed two types of patterns, a central, annular region with no propellant wetting and a peripheral, annular region with wetting, suggestive of various species characterized by their tendency to desorb or deposit onto the beam target surface, respectively.

VI. Conclusion and Path Forward

The UCLA PESPL has developed an end-to-end electrospray modeling framework for investigating the wide-ranging physics and chemistry of plume evolution. By generating a model surrogate, the Propagation of Electrospray Plume Particles in the Exhaust Region (PEPPER) model can greatly reduce the computational cost of estimating design-scale quantities of interest, including grid impingement and thrust. Bayesian inference will be used to determine the likely input conditions that result in the experimentally observed mass flux profiles at the UCLA PESPL. Furthermore, mass flux and current density mapping functions will be presented. Expected conclusions from this study will inform UCLA PESPL's lifetime models [7, 49] and the overall impact of plume expansion on thruster performance. By employing forward and backward propagation frameworks, the PEPPER model will use both higher-fidelity models and experimental measurements to rapidly explore and confine the trade space for designing mission-enabling electrospray thrusters. Future work will investigate how Gaussian mixtures directly quantify the dissimilar species clearly evident in electrospray plume experimental measurements.

Acknowledgments

The authors thank Dr. Colleen Marrese-Reading, Steven Arrestie, and Dr. John Ziemer from NASA JPL and Nathaniel Demmons of Busek Co. Inc. for their insightful discussions. The authors also thank Dr. Ani Thuppu, McKenna Davis Breddan, Henry Huh, Dr. Nolan Uchizono, Peter Wright, and Patrick Crandall for their insightful discussions. This material is based upon work supported by the U.S. Department of Energy, Office of Science, Office of

Advanced Scientific Computing Research, Department of Energy Computational Science Graduate Fellowship under Award Number DE-SC0022158. This work was also funded by NASA/JPL Award No. 1580267 and Air Force Office of Scientific Research Award No. FA9550-21-1-0067.

References

- [1] Hruby, V., Spence, D., Demmons, N., Roy, T., Ehrbar, E., Zwahlen, J., Martin, R., Ziemer, J., Connolly, W., Rhodes, S., and Tolman, W., “ST7-DRS Colloid Thruster System Development and Performance Summary,” *44th AIAA/ASME/SAE/ASEE Joint Propulsion Conference & Exhibit*, Joint Propulsion Conferences, American Institute of Aeronautics and Astronautics, 2008. <https://doi.org/doi:10.2514/6.2008-4824>, URL <https://doi.org/10.2514/6.2008-4824>.
- [2] Ziemer, J. K., “Performance of Electrospray Thrusters,” *31st International Electric Propulsion Conference*, Ann Arbor, MI, USA, 2009, p. pp. 1–13.
- [3] Racca, G. D., and McNamara, P. W., “The LISA Pathfinder Mission,” *Space Science Reviews*, Vol. 151, No. 1, 2010, pp. 159–181. <https://doi.org/10.1007/s11214-009-9602-x>, URL <https://doi.org/10.1007/s11214-009-9602-x>.
- [4] Demmons, N. R., Lamarre, N., Ziemer, J. K., Parker, M., and Spence, D., “Electrospray Thruster Propellant Feedsystem for a Gravity Wave Observatory Mission,” *52nd AIAA/SAE/ASEE Joint Propulsion Conference*, AIAA Propulsion and Energy Forum, American Institute of Aeronautics and Astronautics, 2016. <https://doi.org/doi:10.2514/6.2016-4739>, URL <https://doi.org/10.2514/6.2016-4739>.
- [5] Mennesson, B., “Habitable Exoplanet Observatory Final Report,” Tech. rep., NASA Jet Propulsion Laboratory, NASA Jet Propulsion Laboratory, Pasadena, California, 2019.
- [6] Amaro-Seoane, P., Audley, H., Babak, S., Baker, J. M., Barausse, E., Bender, P. L., Berti, E., Binétruy, P., Born, M., Bortoluzzi, D., Camp, J. B., Caprini, C., Cardoso, V., Colpi, M., Conklin, J. W., Cornish, N. J., Cutler, C., Danzmann, K., Dolesi, R., Ferraioli, L., Ferroni, V., Fitzsimons, E. D., Gair, J. R., Boté, L. G., Giardini, D., Gibert, F., Grimani, C., Halloin, H., Heinzel, G., Hertog, T., Hewitson, M., Holley-Bockelmann, K., Hollington, D., Hueller, M., Inchauspe, H., Jetzer, P., Karnesis, N., Killow, C. J., Klein, A., Klipstein, B., Korsakova, N. K., Larson, S. L., Livas, J. C., Lloro, I., Man, N., Mance, D., Martino, J., Mateos, I., Mckenzie, K., McWilliams, S. T., Miller, C., Mueller, G., Nardini, G., Nelemans, G. A., Nofrarías, M., Petiteau, A., Pivato, P., Plagnol, E., Porter, E. K., Reiche, J., Robertson, D. L., Robertson, N. A., Rossi, E. M., Russano, G., Schutz, B. F., Sesana, A., Shoemaker, D. P., Slutsky, J., Sopuerta, C. F., Sumner, T. J., Tamanini, N., Thorpe, I. J., Troebs, M., Vallisneri, M., Vecchio, A., Vetrugno, D., Vitale, S., Volonteri, M., Wanner, G., Ward, H., Wass, P. J., Weber, W. J., Ziemer, J. K., and Zweifel, P., “Laser Interferometer Space Antenna,” Tech. rep., 2012.
- [7] Thuppul, A., Wright, P. L., Collins, A. L., Ziemer, J. K., and Wirz, R. E., “Lifetime Considerations for Electrospray Thrusters,” *Aerospace*, Vol. 7, No. 8, 2020. <https://doi.org/10.3390/aerospace7080108>.
- [8] Gamero-Castaño, M., “Characterization of the electrosprays of 1-ethyl-3-methylimidazolium bis(trifluoromethylsulfonyl) imide in vacuum,” *Physics of Fluids*, Vol. 20, No. 3, 2008. <https://doi.org/10.1063/1.2899658>.
- [9] Thuppul, A., Collins, A. L., Wright, P. L., Uchizono, N. M., and Wirz, R. E., “Mass flux and current density distributions of electrospray plumes,” *Journal of Applied Physics*, Vol. 130, No. 10, 2021, p. 103301. <https://doi.org/10.1063/5.0056761>, URL <https://doi.org/10.1063/5.0056761>.
- [10] Prince, B. D., Tiruppathi, P., Bemish, R. J., Chiu, Y.-H., and Maginn, E. J., “Molecular Dynamics Simulations of 1-Ethyl-3-methylimidazolium Bis[(trifluoromethyl)sulfonyl]imide Clusters and Nanodrops,” *The Journal of Physical Chemistry A*, Vol. 119, No. 2, 2015, pp. 352–368. <https://doi.org/10.1021/jp507073e>, URL <https://doi.org/10.1021/jp507073e>.
- [11] Iribarne, J. V., and Thomson, B. A., “On the evaporation of small ions from charged droplets,” *The Journal of Chemical Physics*, Vol. 64, No. 6, 1976, pp. 2287–2294. <https://doi.org/10.1063/1.432536>, URL <https://aip.scitation.org/doi/abs/10.1063/1.432536>.
- [12] Gamero-Castaño, M., “Electric-Field-Induced Ion Evaporation from Dielectric Liquid,” *Physical Review Letters*, Vol. 89, No. 14, 2002, p. 147602. <https://doi.org/10.1103/PhysRevLett.89.147602>, URL <https://link.aps.org/doi/10.1103/PhysRevLett.89.147602>.
- [13] Coffman, C., “Electrically-Assisted Evaporation of Charged Fluids: Fundamental Modeling and Studies on Ionic Liquids,” Ph.D. thesis, Massachusetts Institute of Technology, 2016. URL <http://dspace.mit.edu/handle/1721.1/7582>.
- [14] Gu, W., Heil, P. E., Choi, H., and Kim, K., “Comprehensive model for fine Coulomb fission of liquid droplets charged to Rayleigh limit,” *Applied Physics Letters*, Vol. 91, No. 6, 2007, p. 64104. <https://doi.org/10.1063/1.2767774>, URL <https://doi.org/10.1063/1.2767774>.

- [15] Hekmat, M. H., Rahmanpour, M., Mahmoudi, M., and Saharkhiz, S., “A genetic algorithm-based approach for numerical solution of droplet status after Coulomb fission using the energy conservation method,” *Journal of Computational Applied Mechanics*, Vol. 51, No. 2, 2020, pp. 454–463. <https://doi.org/10.22059/JCAMECH.2020.304872.523>.
- [16] Deng, W., and Gomez, A., “Influence of space charge on the scale-up of multiplexed electrosprays,” *Journal of Aerosol Science*, Vol. 38, No. 10, 2007, pp. 1062–1078. [https://doi.org/https://doi.org/10.1016/j.jaerosci.2007.08.005](https://doi.org/10.1016/j.jaerosci.2007.08.005), URL <http://www.sciencedirect.com/science/article/pii/S0021850207001358>.
- [17] Grifoll, J., and Rosell-Llompart, J., “Efficient Lagrangian simulation of electrospray droplets dynamics,” *Journal of Aerosol Science*, Vol. 47, 2012, pp. 78–93. <https://doi.org/10.1016/j.jaerosci.2012.01.001>, URL <http://dx.doi.org/10.1016/j.jaerosci.2012.01.001>.
- [18] Davis, M. J., Collins, A. L., and Wirz, R. E., “Electrospray Plume Evolution Via Discrete Simulations,” *36th International Electric Propulsion Conference*, Vienna, Austria, 2019.
- [19] Gamero-Castaño, M., “Energy dissipation in electrosprays and the geometric scaling of the transition region of cone-jets,” *Journal of Fluid Mechanics*, Vol. 662, 2010, pp. 493–513. <https://doi.org/DOI:10.1017/S0022112010003423>, URL <https://www.cambridge.org/core/article/energy-dissipation-in-electrosprays-and-the-geometric-scaling-of-the-transition-region-of-cone-jets/7CFA007BFDD4A06EC20F6F9BFF04D80F>.
- [20] Huh, H., and Wirz, R., “Numerical Simulation of Electrospray Thruster Extraction,” *36th International Electric Propulsion Conference*, Vienna, Austria, 2019.
- [21] Uchizono, N. M., Collins, A. L., Marrese-Reading, C., Arese, S. M., Ziemer, J. K., and Wirz, R. E., “The role of secondary species emission in vacuum facility effects for electrospray thrusters,” *Journal of Applied Physics*, Vol. 130, No. 14, 2021. <https://doi.org/10.1063/5.0063476>.
- [22] Wirz, R. E., Collins, A. L., Thuppul, A., Wright, P. L., Uchizono, N. M., Huh, H., Davis, M. J., Ziemer, J. K., and Demmons, N. R., “Electrospray Thruster Performance and Lifetime Investigation for the LISA Mission,” *AIAA Propulsion and Energy 2019 Forum*, AIAA Propulsion and Energy Forum, American Institute of Aeronautics and Astronautics, 2019. URL <https://doi.org/10.2514/6.2019-3816>.
- [23] Arridge, S., Maass, P., Öktem, O., and Schönlieb, C.-B., “Solving inverse problems using data-driven models,” *Acta Numerica*, Vol. 28, 2019, pp. 1–174. <https://doi.org/DOI:10.1017/S0962492919000059>, URL <https://www.cambridge.org/core/article/solving-inverse-problems-using-datadriven-models/CE5B3725869AEAF46E04874115B0AB15>.
- [24] Jackson, C., Sen, M. K., and Stoffa, P. L., “An Efficient Stochastic Bayesian Approach to Optimal Parameter and Uncertainty Estimation for Climate Model Predictions,” *Journal of Climate*, Vol. 17, No. 14, 2004, pp. 2828–2841. [https://doi.org/10.1175/1520-0442\(2004\)017<2828:AESBAT>2.0.CO;2](https://doi.org/10.1175/1520-0442(2004)017<2828:AESBAT>2.0.CO;2), URL https://journals.ametsoc.org/view/journals/clim/17/14/1520-0442_2004_017_2828_aesbat_2.0.co_2.xml.
- [25] Byrne, M. P., Jorns, B. A., and Arbor, A., “Data-driven Models for the Effects of Background Pressure on the Operation of Hall Thrusters,” *Presented at the 36th International Electric Propulsion Conference University of Vienna, Austria*, 2019, pp. 2019–630.
- [26] Gamero-Castaño, M., “Characterization and modeling of colloid thruster beams,” *Collection of Technical Papers - AIAA/ASME/SAE/ASEE 42nd Joint Propulsion Conference*, Vol. 4, No. July, 2006, pp. 3256–3261. <https://doi.org/10.2514/6.2006-4643>.
- [27] Gamero-Castaño, M., “Characterization of the electrosprays of 1-ethyl-3-methylimidazolium bis(trifluoromethylsulfonyl) imide in vacuum,” *Physics of Fluids*, Vol. 20, No. 3, 2008, p. 32103. <https://doi.org/10.1063/1.2899658>, URL <https://doi.org/10.1063/1.2899658>.
- [28] Gamero-Castaño, M., and Cisquella-Serra, A., “Electrosprays of highly conducting liquids: A study of droplet and ion emission based on retarding potential and time-of-flight spectrometry,” *Physical Review Fluids*, Vol. 6, No. 1, 2021, pp. 1–20. <https://doi.org/10.1103/physrevfluids.6.013701>.
- [29] GAÑÁN-CALVO, A. M., “On the general scaling theory for electrospraying,” *Journal of Fluid Mechanics*, Vol. 507, 2004, pp. 203–212. <https://doi.org/DOI:10.1017/S0022112004008870>, URL <https://www.cambridge.org/core/article/on-the-general-scaling-theory-for-electrospraying/32BA3083193B3B246663D07516F6E0E8>.
- [30] Parmar, S. M., Collins, A. L., and Wirz, R. E., “Electrospray Plume Modeling for Rapid Life and Performance Analysis,” *AIAA SciTech Forum*, American Institute of Aeronautics and Astronautics, San Diego, CA, 2021. URL <https://doi.org/10.2514/6.2022-1357>.

- [31] Sudret, B., “Global sensitivity analysis using polynomial chaos expansions,” *Reliability Engineering & System Safety*, Vol. 93, No. 7, 2008, pp. 964–979. <https://doi.org/10.1016/j.ress.2007.04.002>, URL <https://www.sciencedirect.com/science/article/pii/S0951832007001329>.
- [32] Shen, D., Wu, H., Xia, B., and Gan, D., “Polynomial Chaos Expansion for Parametric Problems in Engineering Systems: A Review,” *IEEE Systems Journal*, Vol. 14, No. 3, 2020, pp. 4500–4514. <https://doi.org/10.1109/JSYST.2019.2957664>.
- [33] Acar, E., Bayrak, G., Jung, Y., Lee, I., Ramu, P., and Ravichandran, S. S., “Modeling, analysis, and optimization under uncertainties: a review,” *Structural and Multidisciplinary Optimization*, 2021. <https://doi.org/10.1007/s00158-021-03026-7>, URL <https://doi.org/10.1007/s00158-021-03026-7>.
- [34] Kerr, D., “Sensitivity Analysis and Uncertainty Quantification in Reduced-Order Monopropellant Catalyst Bed Model,” Ph.D. thesis, University of California, Los Angeles, 2019.
- [35] Hadigol, M., and Doostan, A., “Least squares polynomial chaos expansion: A review of sampling strategies,” *Computer Methods in Applied Mechanics and Engineering*, Vol. 332, 2018, pp. 382–407. [https://doi.org/https://doi.org/10.1016/j.cma.2017.12.019](https://doi.org/10.1016/j.cma.2017.12.019), URL <https://www.sciencedirect.com/science/article/pii/S0045782517307697>.
- [36] Feinberg, J., and Langtangen, H. P., “Chaospy: An open source tool for designing methods of uncertainty quantification,” *Journal of Computational Science*, Vol. 11, 2015, pp. 46–57. <https://doi.org/https://doi.org/10.1016/j.jocs.2015.08.008>, URL <https://www.sciencedirect.com/science/article/pii/S1877750315300119>.
- [37] Sivia, D. S., and Skilling, J. J., *Data analysis a Bayesian tutorial*, 2nd ed., Oxford University Press, Oxford, 2006.
- [38] Salvatier, J., Wiecki, T. V., and Fonnesbeck, C., “Probabilistic programming in Python using PyMC3,” *PeerJ Computer Science*, Vol. 2, 2016, p. e55. <https://doi.org/10.7717/peerj-cs.55>, URL <https://doi.org/10.7717/peerj-cs.55>.
- [39] Diebolt, J., and Robert, C. P., “Estimation of Finite Mixture Distributions through Bayesian Sampling,” *Journal of the Royal Statistical Society. Series B (Methodological)*, Vol. 56, No. 2, 1994, pp. 363–375. URL <http://www.jstor.org/stable/2345907>.
- [40] Richardson, S., and Green, P. J., “On Bayesian Analysis of Mixtures with an Unknown Number of Components (with discussion),” *Journal of the Royal Statistical Society: Series B (Statistical Methodology)*, Vol. 59, No. 4, 1997, pp. 731–792. <https://doi.org/https://doi.org/10.1111/1467-9868.00095>, URL <https://doi.org/10.1111/1467-9868.00095>.
- [41] Escobar, M. D., and West, M., “Bayesian Density Estimation and Inference Using Mixtures,” *Journal of the American Statistical Association*, Vol. 90, No. 430, 1995, pp. 577–588. <https://doi.org/10.1080/01621459.1995.10476550>, URL <https://www.tandfonline.com/doi/abs/10.1080/01621459.1995.10476550>.
- [42] Wilson, R., “MGMM: multiresolution Gaussian mixture models for computer vision,” *Proceedings 15th International Conference on Pattern Recognition. ICPR-2000*, Vol. 1, 2000, pp. 212–215. <https://doi.org/10.1109/ICPR.2000.905305>.
- [43] Štěpánek, M., Franc, J., and Kůs, V., “Modification of Gaussian mixture models for data classification in high energy physics,” *Journal of Physics: Conference Series*, Vol. 574, 2015, p. 12150. <https://doi.org/10.1088/1742-6596/574/1/012150>, URL <http://dx.doi.org/10.1088/1742-6596/574/1/012150>.
- [44] Garcia, V., Nielsen, F., and Nock, R., “Levels of Details for Gaussian Mixture Models BT - Computer Vision – ACCV 2009,” Springer Berlin Heidelberg, Berlin, Heidelberg, 2010, pp. 514–525.
- [45] GAMERO-CASTAÑO, M., and HRUBY, V., “Electric measurements of charged sprays emitted by cone-jets,” *Journal of Fluid Mechanics*, Vol. 459, 2002, pp. 245–276. <https://doi.org/DOI:10.1017/S002211200200798X>, URL <https://www.cambridge.org/core/article/electric-measurements-of-charged-sprays-emitted-by-conejets/DDB2A0EA0BCC0625342E61FAC68FA071>.
- [46] Collins, A. L., Wright, P. L., Uchizono, N. M., and Wirz, R. E., “Neutral Mass Flux Measurements of an Electrospray Plume,” *International Electric Propulsion Conference*, ERPS, 2022, p. 227.
- [47] Uchizono, N. M., Collins, A. L., Marrese-Reading, C., Arrestie, S. M., Ziemer, J. K., and Wirz, R. E., “Positive and negative secondary species emission behavior for an ionic liquid electrospray,” *Applied Physics Letters (In Review)*, 2022.
- [48] Uchizono, N. M., Wright, P. L., Collins, A. L., Chamieh, M. C., Chandrasekar, K., and Wirz, R. E., “Electrospray Thruster Facility Effects: Characterization and Mitigation,” *International Electric Propulsion Conference*, ERPS, 2022, p. 219.
- [49] Collins, A. L., Thuppul, A., Wright, P. L., Uchizono, M., Nolan, Huh, H., Davis, M. J., Ziemer, J. K., Demmons, N. R., and Wirz, R. E., “Assessment of Grid Impingement for Electrospray Thruster Lifetime,” *36th International Electric Propulsion Conference*, Vienna, Austria, 2019.